Earth and Planetary Science Letters 538 (2020) 116195

Contents lists available at ScienceDirect

Earth and Planetary Science Letters

www.elsevier.com/locate/epsl

Thick, strong sediment subduction along south-central Chile and its role in great earthquakes

Kelly M. Olsen [a,*], Nathan L. Bangs [a], Anne M. Tréhu [b], Shuoshuo Han [a], Adrien Arnulf [a], Eduardo Contreras-Reyes [c]

[a] Institute for Geophysics, University of Texas, 10601 Exploration Way, Austin, TX 78758, USA
[b] College of Earth, Ocean, and Atmospheric Sciences, Oregon State University, 104 CEOAS Admin Building, 101 Southwest 26th Street, Corvallis, OR 97331, USA
[c] Departamento de Geofísica, Facultad de Ciencias Físicas y Matemáticas, Universidad de Chile, 8370449 Santiago, Chile

ARTICLE INFO

Article history:
Received 4 November 2019
Received in revised form 19 February 2020
Accepted 28 February 2020
Available online 16 March 2020
Editor: J.-P. Avouac

Keywords:
Chile
earthquake
trench
sediment
decollement
subduction

ABSTRACT

The south-central Chile margin experienced the largest and sixth largest earthquakes ever recorded - the 1960 Mw 9.5 Valdivia and 2010 Mw 8.8 Maule megathrust earthquakes, respectively. In early 2017, we conducted a seismic survey along 1,000 km of south-central Chile to image these rupture zones using a 15.15-km-long multi-channel seismic streamer. We processed these data using pre-stack depth migration, which provides the best look at the shallow part of the south-central Chile margin to date. Relative to other sediment-dominated subduction zones, where sediment is typically accreted at the toe, an unusually large percentage of the thick trench sediments are consistently subducted beneath the slope with little thrust faulting or deformation. Analysis of the sediment P-wave velocities and structure in the trench and outer wedge leads us to conclude that most of south-central Chile contains well-drained, strong sediments. An exception in the vicinity of the subducting Mocha Fracture Zone (MFZ) has trench sediments that appear to experience localized delayed compaction, thus lowering their strength and allowing the development of protothrusts, similar to what is seen in other accretionary subduction zones. The very shallow décollement along the south-central Chile allows more sediment to pass beneath the lower slope than almost all other subduction zone, many of which have much thicker trench sections. We conclude that subduction of the strong, well-drained, thick sediment layer beneath the lower slope is typical for nearly all of the south-central Chile. Comparison to other thick-sedimented subduction zones worldwide reveals that the subduction of such a large fraction of the trench sediment is particularly unusual. This strong, thick, subducting sediment is likely a determining factor for developing a smooth plate interface located well above the subducted crust topography that ultimately becomes a broad megathrust with high, homogeneous frictional properties, and generates particularly large earthquakes along the south central Chile margin.

1. Introduction

Many of the world's largest and most destructive earthquakes occur along subduction zone megathrusts, particularly ones that develop a smooth, homogeneous plate interface that allows broad areas of strong plate locking and large strain accumulation (e.g. Ruff, 1989; Scholl et al., 2015). Consequently, great earthquakes are strongly correlated with subduction zones characterized by long segments within which the thickness of trench sediment immediately seaward of the deformation front is >1 km for hundreds of kilometers (Ruff, 1989; Heuret et al., 2012; Scholl et al., 2015; Ye et al., 2018). This relationship has been attributed to sediment that is thick enough to bury the basement topography of the subducting crystalline crust, thus allowing the megathrust to form a smooth homogeneous plate boundary (Contreras-Reyes and Carrizo, 2011; Wang and Bilek, 2014). Ultimately, it is the position of the décollement within the trench sediment section that determines how much of the trench sediment is removed, primarily by accretion at the deformation front, and whether topography on the subducted plate produces roughness on the plate boundary. The development of the décollement is affected by weak lithologies within trench sediments, (e.g. high smectite content; Kopf and Brown, 2003) or high pore-fluid pressures (e.g. Bangs et al., 2004, 2009, 1990; Bray et al., 1986; Dean et al., 2010; Geersen et al., 2013; Hüpers et al., 2017) that often tend to lie within the lower pelagic units rather than overlying trench fill sequences. With the

* Corresponding author.
E-mail address: kolsen@utexas.edu (K.M. Olsen).

https://doi.org/10.1016/j.epsl.2020.116195
0012-821X/

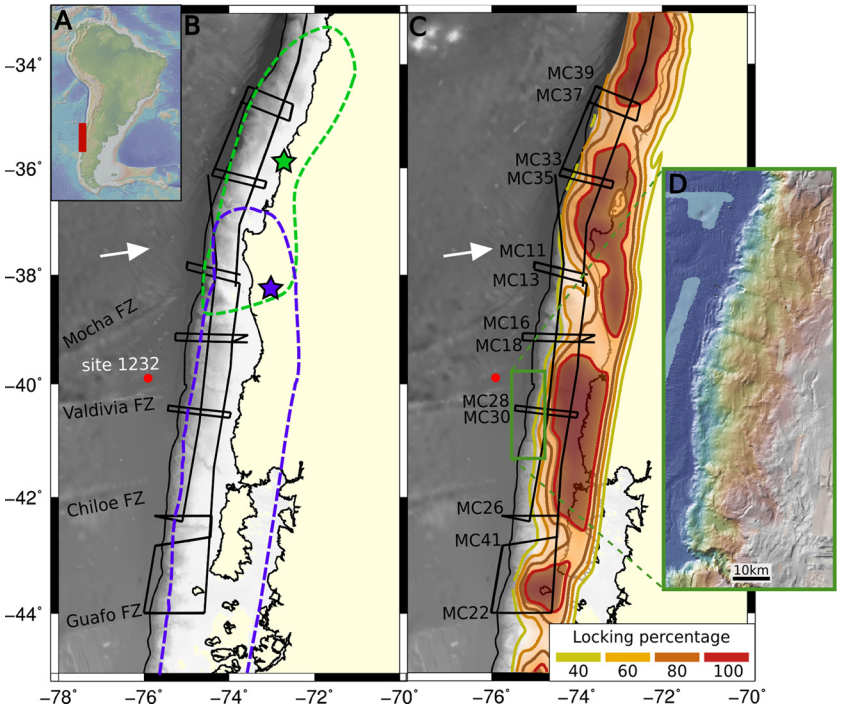

Fig. 1. Study area A) Location of CEVICHE survey. B) Dashed lines shows the rupture segment of the 1960 Mw 9.5 Valdivia earthquake (Moreno et al., 2009) (purple) and the 2010 Mw 8.8 Maule earthquake (Moreno et al., 2010) (green). Black lines show CEVICHE multichannel seismic data lines. Red circle shows ODP site 1232 (Mix et al., 2003). C) Contours show the interplate locking (Moreno et al., 2009, 2010, 2011). D) Subset of bathymetry along the margin showing the chaotic structure of the wedge and the absence of long, continuous thrust ridges. (For interpretation of the colors in the figure(s), the reader is referred to the web version of this article.)

exception of local or regional effects from subducting seamounts or other basement structures (e.g. Bangs et al., 2006; Contreras-Reyes and Carrizo, 2011; Moore et al., 2009; Morgan and Bangs, 2017; Tréhu et al., 2012), the décollement commonly forms within the lower half of the incoming trench sediments and removes a large fraction (>50%) of the subducting sediment cover at the deformation front (e.g. Barnes et al., 2018; Dean et al., 2010; Eakin, 2014; Han et al., 2017; Kopp et al., 2000; Li et al., 2018; Moore et al., 2009, 1990; Nasu et al., 1982). In these instances, a thick, smooth, laterally continuous plate boundary may not form as readily.

The south central Chile margin regularly experiences large earthquakes and is the site of the 1960 Mw 9.5 Valdivia earthquake, which is the largest earthquake recorded by global networks (Cifuentes, 1989; Contreras-Reyes and Carrizo, 2011). The Valdivia earthquake ruptured ~950 km of the margin north of the Chile Triple Junction (Moreno et al., 2009; Plafker and Savage, 1970) (Fig. 1A). The 2010 Mw8.8 Maule earthquake ruptured a ~500 km segment south of the Juan Fernández Ridge, overlapping spatially with the Valdivia rupture (Moreno et al., 2010). Geodetic interplate locking models from GPS observed from 1996 to 2008 (Fig. 1B) show that large portions of the margin are fully locked (i.e. where plate coupling is >80%) during the inter-seismic period (Moreno et al., 2011, 2010, 2009).

In this manuscript, we present new, pre-stack depth migrated seismic reflection images of recently-acquired seismic data as part of the CEVICHE (Crustal Examination from Valdivia to Illapel to Characterize Huge Earthquakes) project, and velocity models along selected 2D transects from the incoming plate and sediments across the deformation front and into the outer wedge. The results from analysis of deformation structures within the trench and lower continental slope in these new data show that sediment thickness in the trench is ~1.6–2.9 km, and that the décollement forms at an unusually shallow level near the top of the thick incoming trench sediment wedge along all of the Valdivia and southern portions of the Maule rupture areas. Prior reflection surveys of south-central Chile have shown variability in the depth of the décollement at the deformation front and in the partitioning of incoming sediment between accretion and subduction (Bangs and Cande, 1997; Behrmann and Kopf, 2001; Díaz-Naveas, 1999; Contreras-Reyes et al., 2010; Geersen et al., 2011; Tréhu et al., 2019). The CEVICHE dataset shows that sediment subduction, as opposed to frontal accretion or erosion, is the dominant process along these rupture segments. The development of an unusually shallow décollement along south-central Chile results in underthrust sediment thickness that is more than double that at most other margins (Table 1). We also show evidence based on seismic velocities that this is a result of trench and underthrust sediments that are well-consolidated and strong, which may also help maintain a shallow décollement and a thick, frictionally strong, underthrust section down dip into the seismogenic zone. The goal of this study is to show that the south central Chile margin has very little frontal accretion in comparison to other well-sedimented subduction zones and a particularly thick, broad sediment section subducts beneath the lower slope. This is significant for south-central Chile as an initial step toward developing a broad, smooth homogeneous megathrust that can store large stress and rupture in large earthquakes (e.g. Scholl et al., 2015).

2. Seismic data acquisition and processing

In early 2017, we acquired 4,867 km of 2D seismic reflection data along south-central Chile as part of the CEVICHE project (Fig. 1). Seismic sources generated by a 6,600 in^3 (108 L) airgun array were recorded on a 15.15-km, 1212-channel hydrophone streamer towed by the *R/V Marcus G. Langseth*. Due to the long source-receiver offsets relative to target depths, the streamer was long enough to record deep-turning refraction arrivals and high-quality reflections in a wide range of normal moveout that accurately constrain seismic P-wave velocities (see Supplemental Files for uncertainty estimation). The common midpoint spacing of the data is 6.25 m and shots were fired every 50 m. We measured interval velocities with depth for each of the lines using stack-

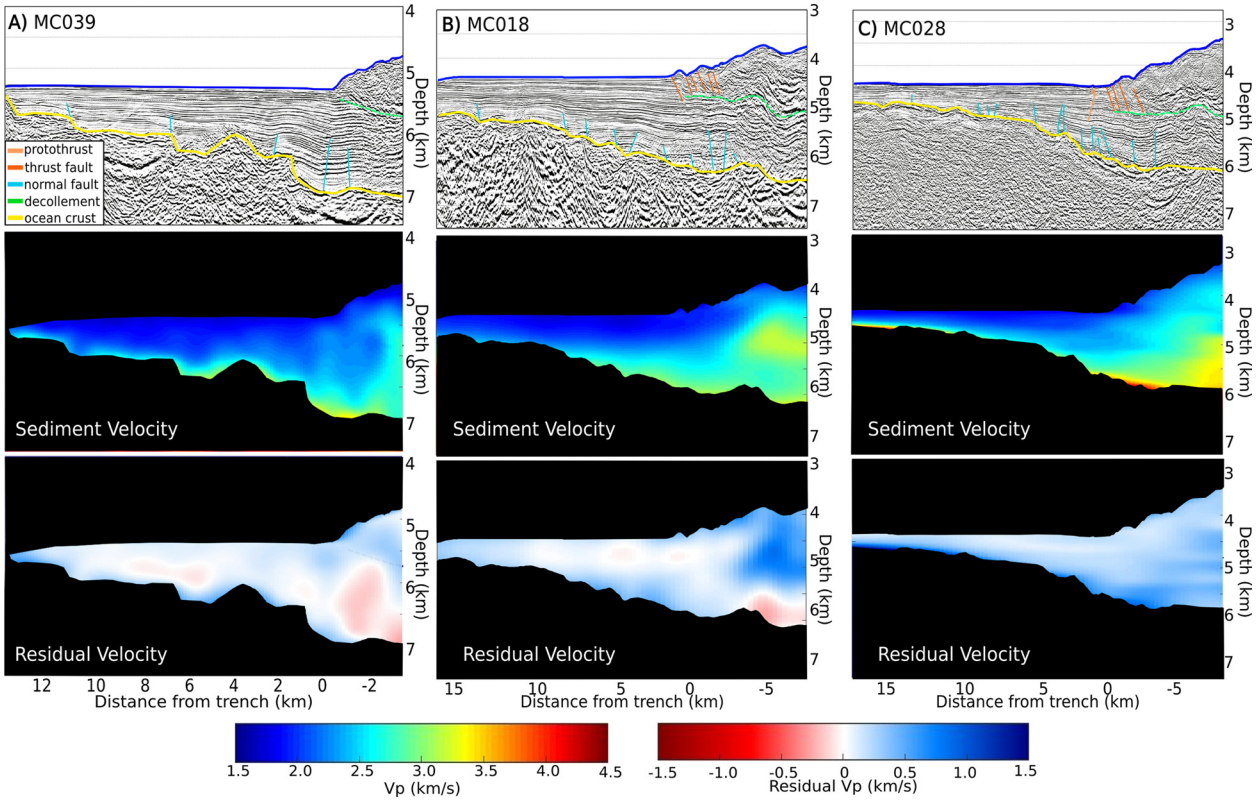

Fig. 2. Pre-stack depth migrated images and interpretations, interval velocity model, and residual velocity for A) line 039, located ~34.5°S, B) line 018, located ~39.2°S, and C) line 028, located ~40.3°S. Thrust faults are shown in orange on the interpretation, protothrusts in light orange, normal faults in blue, ocean crust in yellow, and the décollement in green. Uninterpreted images extending to 10 km landward of the trench are presented in the Supplemental Material.

ing velocity analysis as a starting model. Velocities were iteratively updated following residual velocity analysis during depth imaging using Kirchhoff pre-stack depth migration. On two lines, MC13 and MC18, we also derived velocities from tomographic inversions of picked first arrivals from the streamer data after downward continuation to the seafloor (Arnulf et al., 2018, 2011).

3. Results

3.1. Seismic structure

To characterize the décollement, we selected and analyzed a subset of the CEVICHE lines (Figs. 2 and 3) that shows representative examples of the deformation front adjacent to the Maule and Valdivia rupture zones. This region is characterized by a range in plate locking (Fig. 1), variation in trench sediment thickness (Fig. 5), and changes in frontal deformation structures (all frontal zones from CEVICHE are shown in the supplement, Supplemental Figs. 4–16). These data show considerable structural complexity across the deformation front with some indications of frontal accretion, such as faulted and folded strata (Fig. 2B), or shallow underplating, such as truncated reflections (Fig. 2A). Although streamer feathering and scattering from complex seafloor bathymetry increase the noise level of the images, the décollement can be determined to be very shallow. The décollement does not produce a strong seismic reflection, as is commonly observed along other margins (e.g. Moore et al., 1990); however, it can still be identified by the contrast between the reflection character of the wedge (chaotic, discontinuous, dipping reflections) and that of the underthrust sediments (laterally-continuous, sub-horizontal layered sequences; Figs. 2–4). The continuity of the undeformed, underthrust trench strata shows that nearly all of the sediment within the trench has bypassed the toe of the accretionary wedge

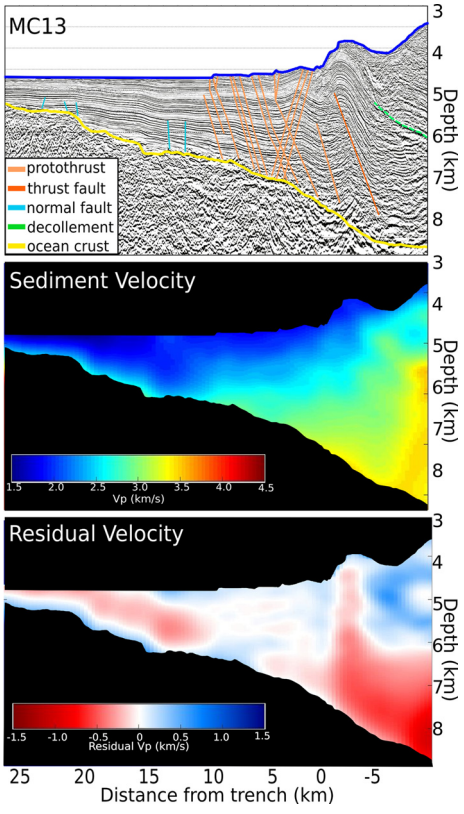

Fig. 3. Pre-stack depth migrated image and interpretations, interval velocity model, and residual velocity for line 013, located ~38°S. This is one of two lines showing anomalous thrusting and velocities along the margin. Interpretation is the same as for Fig. 2. Uninterpreted images extending to 10 km landward of the trench are presented in the Supplemental Material.

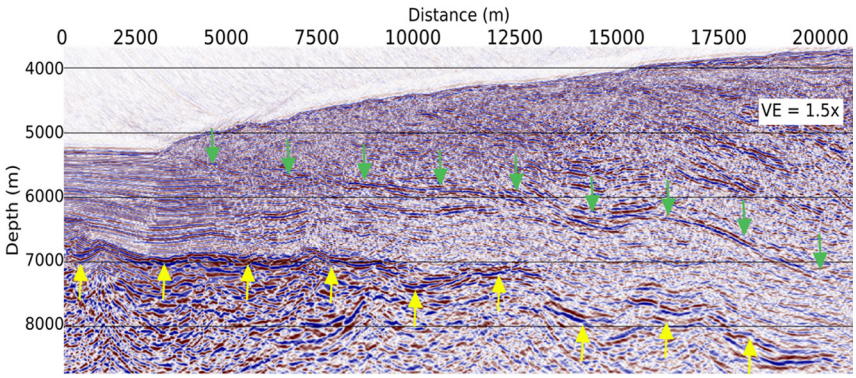

Fig. 4. Line MC39 showing sediment subducting in the Maule segment to >20 km from the deformation front. Yellow arrows show the top of the oceanic basement, while green arrows show the décollement reflector, with sediment subducting in between. This contrasts some previous studies that have suggested that the Maule segment is dominated by frontal sediment accretion (Bangs and Cande, 1997; Sick et al., 2006).

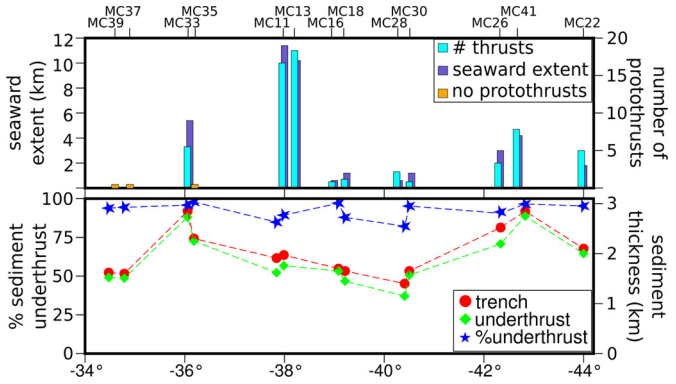

Fig. 5. Top: Number of thrusts (blue) and seaward extent of thrust faults, measured from the trench axis (purple). Orange squares mark where no thrusts faults prior to the main frontal thrust are observed seismically. Bottom: Sediment thickness measured just seaward of the deformation front (red circles) and in the underthrust section ~10 km east of the trench (green diamonds). Percent sediment that is underthrust beneath the toe along the margin is shown with blue stars.

(Figs. 2–4, Supplemental Figs. 4–16). The plate boundary in south-central Chile forms at a very shallow position in all of the 13 CEVICHE profiles across the trench, allowing ~80–95% of the trench sediment to subduct beneath the toe and frontal wedge (Figs. 2–5; Supplemental Figs. 4–16).

Along with the shallow décollement, we see little deformation within the trench sediment associated with the deformation front. All of the lines show low-offset (<20 m) normal faults in the incoming sediments that we attribute to plate bending (blue lines on Figs. 2 and 3). These normal faults dip ~65–75° and extend from the oceanic basement through the lower ~1/3 of the trench sediments but do not typically intersect recently deposited sediments near the seafloor. A second, independent set of faults are low-vertical displacement thrusts that form seaward of the main frontal deformation with dips between ~40–50°. Prototthrusts are generally defined to be small offset thrust faults observed seaward of the large displacement thrust fault that defines the deformation front (e.g. Barnes et al., 2018; Cochrane et al., 1994; Moore et al., 1990) and are interpreted to define areas of compaction in the trench sediments (Barnes et al., 2018; Bray et al., 1986). On nearly all of the CEVICHE profiles, there are relatively few thrusts and they exhibit complex relationships. Here we identify "prototthrusts" as thrust faults with displacement <30 m that lie seaward of the high strain regions of the accretionary wedge, which has thickened by large displacement thrusts that are not well imaged due to the high strain. In any case, they do not extend more than 2–3 km seaward of the high displacement thrust faults that are actively involved in frontal accretion (Fig. 2; Supplemental Figs. 4–16). These observations contrast significantly with observations from other well-sedimented margins such as Nankai (Moore et al., 1990), Hikurangi (Barnes et al., 2018) or Oregon (Cochrane et al., 1994; Han et al., 2017), where prototthrusts form as far as 7.5–12 km seaward of the deformation front. Along Chile, there is very little evidence of strain propagating into the trench sediment beyond the deformation front.

The only region where the formation of considerable prototthrusts are observed in the seismic data occurs near 38°S in lines MC11 and MC13 (Fig. 3; Supplemental Fig. 8). Fig. 3 shows one of the two profiles (line MC13) where thrusts with larger offsets (>30 m) and conjugate dips (~35–50°) form within the incoming trench section out to ~10 km seaward of the frontal thrust. These prototthrusts extend down to a deep layer near the top of ocean crust; however, the down dip continuity of strata beneath the lower slope implies that the long-term position of the décollement remains shallow, and a deep décollement does not develop. The strain resulting from the prototthrusts appears to be accommodated by internal deformation within the lower strata of the subducting trench sediment, and prototthrusts likely become inactive once they are subducted. The shallow décollement position appears to be stable in this region due to the consistent thickness of continuous subducted sequences, congruous with the thick sediment subduction observed along the rest of the margin.

3.2. Sediment velocity anomalies

Following other studies (e.g. Bangs et al., 1990; Cochrane et al., 1994; Erickson and Jarrard, 1998; Han et al., 2017; Li et al., 2018), we look at P-wave velocities for additional clues to sediment consolidation state and inherent strength. By comparing sediment velocities to a reference velocity curve for normally consolidated distal turbidites (i.e. the offshore Oregon transect presented by Han et al., 2017), we can detect over or under consolidated strata within the incoming sediment section. We use velocities of the undeformed trench sediment along Chile, which are similar to those off Oregon (Han et al., 2017), and conclude that the reference is sufficiently similar that we can use the Han et al. (2017) reference (see Supplemental Material for justification of reference velocity). The residual velocity (observed minus reference velocity) of the incoming sediment in each of our profiles is small across the trench to the deformation front. This includes both regions of the trench that are well seaward of the deformation, which is expected from our reference, as well as regions that are landward of the deformation front. This sharply contrasts with what is seen offshore Oregon, where the thick subducting sediment packet has negative residual velocities both seaward and landward of the deformation front, presumed to be a result of delayed consolidation

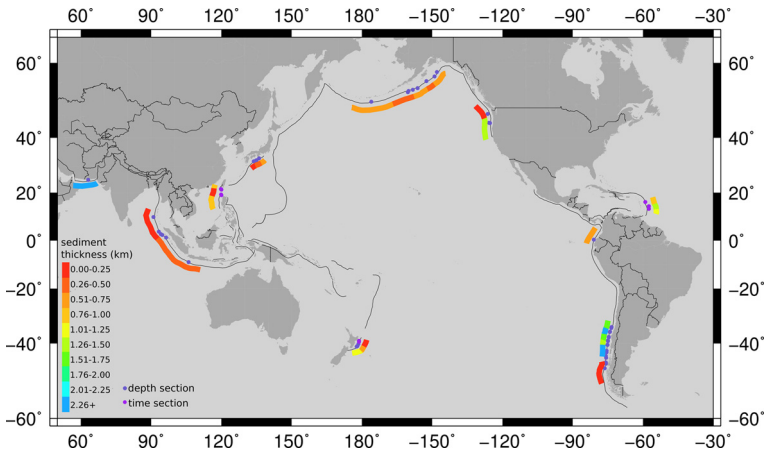

Fig. 6. Thickness of underthrust sediment for thick (>1 km) sedimented subduction zones. The colored values have along the trench have been interpolated from seismic reflection profile measurements, whose locations are shown with dots. Blue dots represent measurements from depth sections; purple are from time sections. Sources found in Table 1.

(Han et al., 2017). Delayed consolidation is also typical along other margins, such as Barbados (Bangs et al., 1990; Bray et al., 1986; Cochrane et al., 1994), Nankai (Bangs et al., 2009), and Alaska (Li et al., 2018). Landward of the trench in south-central Chile, underthrust sediments have small negative residual anomalies that are too low to imply substantial delayed consolidation and possible over-pressuring when compared to other margins (Cochrane et al., 1994; Bangs et al., 1990; Han et al., 2017; Li et al., 2018; Fig. 3).

The only exception to this pattern in our data is near the MFZ on lines MC11 (Supplemental Fig. 8) and MC13 (Fig. 3), where velocities are slower than the reference velocity across the trench. The slow anomalies in the sediments occur seaward of the protothrusts that form on these profiles, increase to near zero within the area of protothrusts, and decreases again in the sediments subducting beneath the wedge. This pattern suggests a region of relatively poorly drained sediment near the MFZ, and that the protothrusts may locally provide drainage pathways to allow some consolidation. Negative residuals within the incoming and underthrust sediment beneath the frontal wedge indicate lower Vp and thus less overall consolidation here than the other CEVICHE profiles, consistent with weaker sediments that are more prone to development of protothrusts. There is no evidence for particularly high stress in this location to cause the protothrusts, and these observations imply stress propagating into south-central Chile trench sediment is only sufficient to develop protothrusts where sediments may be locally somewhat weaker.

4. Discussion

4.1. Global compilation of underthrust sediment thickness at well-sedimented margins

The deformation front is a critical zone for the development of the seismogenic zone. A thick underthrust sediment section relative to basement topography at the toe enhances the development of a smooth and homogeneous plate boundary at seismogenic depths. Scholl et al. (2015) defines thick sediment where the sediment thickness at the deformation front is greater than 1 km. For the thick trenches that Scholl et al. (2015) have identified, we have compiled examples of the sediment subduction fraction from seismic reflection data, based on the authors' decollement interpretations (Fig. 6, Table 1). We attempted to maintain consistency with measurements by using the original authors' decollement measurements instead of reinterpreting the data ourselves, which was often not possible due to the resolution of published figures. Whenever possible, we used depth sections for our measurements. When depth sections were not available, we used time sections and converted the two-way-travel time to depth using a constant velocity of 2 km/s within the sediments (Table 1, highlighted in purple), but we acknowledge an inherent uncertainty. We selected only lines that did not have subducting basement structure, such as seamounts, at the deformation front, as these features may affect the amount of sediment bypassing the toe (i.e. Bangs et al., 2006). The data were compiled from multiple sources for most of the margins, and is intended as a representative, rather than comprehensive, sampling.

The results of the compilation (Fig. 6 and Table 1) show that apart from south-central Chile, no other setting has more than 50% of the incoming sediment subducted beneath the wedge, and <25% is more typical. Except for the extremely thick (7.5 km) Makran setting, underthrust sediment thickness is typically less than 1 km (Kopp et al., 2000). There are localized areas in Cascadia, Barbados, and Hikurangi where >1 km of sediment is subducting past the toe, but as Fig. 6 shows, this does not typically extend for large sections of the margin. Many subduction zones with thick (>1 km) trench sediment sections around the globe develop décollements within pelagic and hemipelagic sections near the base of the trench section; however, the décollement forms in an extremely shallow position within the turbidite sequences in south-central Chile. The compilation shows that the large amount of trench sediment that is typically scraped off the subducting plate makes the frontal zone a critical determining factor for what will eventually be subducted down to the seismogenic zone.

4.2. Thick underthrust sediment section along Chile

One of the most remarkable observations from the CEVICHE dataset is that the décollement forms at an unusually shallow level at the deformation front, near the top of the trench sediments. The shallow décollement along Chile allows the subduction of a thick (>1.5 km) trench section beyond the toe (Fig. 2, 4), despite having only moderate trench sediment thickness (Fig. 6). Where sediment subduction greater than 1 km does occur at other convergent margins, it is localized and likely dependent on a change in lithology, like Cascadia (Han et al., 2017), or due to a subducting seamount or ridge, such as what is hypothesized in Nankai (Bangs et al., 2006), and observed in Alaska (von Huene et al., 2012). The localized sediment accretion that is observed on one seismic line just north of our lines in the Maule rupture area is interpreted by Tréhu et al. (2019) be a temporary process needed to "heal" an embayment in the margin caused by a large topographic feature at least 2 Ma. Otherwise, the shallow décollement forms along the entire

Table 1
Global sediment thickness for thick (>1 km) trenches. Sediment thicknesses were measured from seismic sections, and underthrust thickness is based on author's décollement interpretation. Purple highlighted sites are based on time sections, where a constant 2 km/s was applied to convert time to depth.

Subduction Zone	Thickness subducted	Thickness at DF	Thickness accreted	Percent subducted	Percent accreted	Lat	Long	Source
Makran	3.00	7.50	4.50	0.40	0.60	25.00	63.15	Kopp et al. (2000)
Chile	2.75	2.85	0.10	0.96	0.04	−42.83	−75.53	this study
Chile	2.73	2.85	0.12	0.96	0.04	−36.06	−74.08	this study
Chile	2.43	2.52	0.09	0.96	0.04	−42.34	−75.50	this study
Chile	2.25	2.30	0.05	0.98	0.02	−36.18	−74.18	this study
Chile	2.00	2.10	0.10	0.95	0.05	−44.00	−75.86	this study
Chile	1.76	1.97	0.21	0.89	0.11	−37.99	−74.60	this study
Chile	1.65	1.70	0.05	0.97	0.03	−39.08	−74.96	this study
Chile	1.62	1.91	0.29	0.85	0.15	−37.84	−74.59	this study
Chile	1.57	1.65	0.08	0.95	0.05	−40.50	−75.16	this study
Chile	1.52	1.62	0.10	0.94	0.06	−34.48	−73.39	this study
Chile	1.51	1.60	0.09	0.94	0.06	−34.79	−73.52	this study
Cascadia	1.50	3.40	1.70	0.44	0.50	44.60	−125.30	Han et al. (2017)
Chile	1.45	1.65	0.20	0.88	0.12	−39.22	−74.97	this study
Barbados	1.40	2.90	1.50	0.48	0.52	14.45	−57.50	Bangs et al. (1990)
Cascadia	1.25	3.20	1.95	0.39	0.61	44.70	−125.80	Cochrane et al. (1994)
Chile	1.15	1.40	0.25	0.82	0.18	−40.41	−75.15	this study
Hikurangi	1.10	4.00	2.90	0.28	0.73	−40.80	178.10	Barnes et al. (2018)
Barbados	1.10	2.50	1.60	0.44	0.64	13.40	−57.50	Bangs et al. (1990)
Hikurangi	1.00	3.70	2.70	0.27	0.73	−41.00	177.75	Barnes et al. (2018)
Taiwan	1.00	2.50	1.50	0.40	0.60	19.00	120.00	Eakin (2014)
Barbados	0.90	1.80	0.90	0.50	0.50	16.20	−59.00	Bangs et al. (1990)
Taiwan	0.80	2.30	1.50	0.35	0.65	21.40	119.80	Eakin (2014)
Alaska-Aleutians	0.75	1.75	1.00	0.43	0.57	57.00	−149.00	von Huene et al. (2012)
Alaska-Aleutians	0.90	2.30	1.45	0.33	0.63	54.20	−156.25	Li et al. (2018)
Hikurangi	0.60	3.80	3.20	0.16	0.84	−40.20	178.50	Barnes et al. (2018)
Alaska-Aleutians	0.60	2.00	1.40	0.30	0.70	58.00	−148.00	von Huene et al. (2012)
Nankai	0.60	2.40	1.80	0.25	0.75	33.00	136.10	Moore et al. (2009)
Colombia	0.52	1.30	0.78	0.40	0.60	0.40	−81.00	Marcaillou et al. (2016)
Sumatra	0.50	4.50	4.00	0.11	0.89	2.40	94.75	Dean et al. (2010)
Sumatra	0.50	4.50	4.00	0.11	0.89	1.30	96.40	Dean et al. (2010)
Alaska-Aleutians	0.50	1.20	0.70	0.42	0.58	53.20	−160.40	von Huene et al. (2019)
Nankai	0.50	1.60	1.10	0.31	0.69	33.20	136.80	Park et al. (2002)
Nankai	0.50	1.00	0.50	0.50	0.50	32.30	135.00	Bangs et al. (2006)
Alaska-Aleutians	0.35	1.40	1.05	0.25	0.75	55.90	−152.47	Davis and von Huene (1987)
Java	0.30	1.30	1.00	0.23	0.77	−9.10	−254.00	Kopp et al. (2009)
Taiwan	0.25	2.20	1.95	0.11	0.89	19.20	119.90	Eakin (2014)
Sumatra	0.20	3.00	2.80	0.07	0.93	2.75	94.15	Gulick et al. (2011)
Cascadia	0.20	3.10	3.10	0.06	1.00	47.30	−126.30	Han et al. (2017)
Sumatra	0.20	2.60	2.40	0.08	0.92	3.80	93.30	Gulick et al. (2011)
Chile	0.00	3.30	3.30	0.00	1.00	−47.58	−76.30	Behrmann and Kopf (2001)
Nankai	0.00	1.40	1.40	0.00	1.00	31.90	133.80	Nasu et al. (1982)
Sumatra	0.00	3.20	3.20	0.00	1.00	10.00	90.00	Moeremans et al. (2014)
Taiwan	0.00	2.75	2.75	0.00	1.00	21.20	120.00	Lester et al. (2013)
Hikurangi	0.00	1.60	1.60	0.00	1.00	−39.17	178.75	Pedley et al. (2010)
Hikurangi	0.00	1.50	1.50	0.00	1.00	−39.42	178.75	Pedley et al. (2010)

~1,000-km-long segment of the Maule and Valdivia rupture areas that we surveyed and along southern portions of the Valdivia rupture that we did not cover (Scherwath et al., 2009; Behrmann and Kopf, 2001). Our observation is also consistent with previous observations that the frontal accretionary prism along south central Chile is small relative to the trench supply since Pliocene (Bangs and Cande, 1997; Contreras-Reyes et al., 2010), and over the long term most of the incoming trench material is subducting beyond the toe and not frontally accreted.

The formation of the shallow décollement along this margin may be explained by trench sediments that drain more readily and are stronger than at other subduction settings. As the trench section approaches and passes beneath the deformation front, it becomes subjected to additional stresses. Along other margins, the result is delayed consolidation as far as 15 km seaward of the trench, as evidenced by drilling results and slow seismic velocities in sediments beneath the décollement and proto-décollement (e.g. Bangs et al., 1990; Cochrane et al., 1994; Han et al., 2017; Li et al., 2018; Moore et al., 2009). Along the section of the Chile margin spanned by our study, with the exception of the MFZ region, residual velocity anomalies are mostly neutral seaward of the trench and only slightly negative beneath the lower slope (Fig. 2; Supplemental Figs. 4–16). We also observe very few thrusts that extend seaward into the trench section. This may be a result of minimal stress propagation from the wedge into the trench section, but it is also consistent with strong resistance to thrusting due to particularly strong sediment or the lack of weak intervals within the trench section. These observations imply that the sediment is well-drained before reaching the deformation front and can drain fast enough to maintain normal consolidation as subduction beneath the lower slope increases overburden. Minimal overpressures form within the subducted sediments in south-central Chile, in contrast to what is seen offshore Oregon (Han et al., 2017), Barbados (Bangs et al., 1990), Nankai (Bangs et al., 2009), and Alaska (Li et al., 2018), where slow velocity layers are observed both beneath the décollement and the proto-décollement.

The low amplitude of the décollement reflection is not a result of poor imaging, as we can see reflections from layers beneath this reflector. Instead it results from the small contrast in density and seismic velocity above and below the décollement. It is thus consistent with the presence of a well-drained, normally consolidated trench section that does not contain excess fluid to be expelled

and trapped along the décollement as a result of subduction. Large impedance contrasts and high amplitude décollements are commonly seen along other margins and are attributed to differences in consolidation across the décollement, where accreted sediments may be over-consolidated (e.g. Morgan and Karig, 1995; Han et al., 2017), and underthrust sediments undergo delayed consolidation (e.g. Moore et al., 1990; Bangs et al., 1990; Cochrane et al., 1994; Han et al., 2017; Li et al., 2018). Our Vp anomalies do not indicate that there is substantial difference in the consolidation of the sediments above and below the décollement (Fig. 2, Supplemental Figs. 4–16).

The hypothesis that the trench sediments drain readily and strengthen enough to resist faulting is verified by our observations within the Mocha Fracture Zone region where this does not occur. Along this segment we find slower Vp and negative Vp anomalies in the incoming sediment section that imply they are poorly drained, and possibly over-pressured (Erickson and Jarrard, 1998) making them inherently weaker (Fig. 3) (Jaeger and Cook, 1969). Coincidentally, we observe a high number of protothrust faults observed on MC13 (Fig. 3) and MC11 (Supplemental Fig. 8). Furthermore, we also see that Vp increases (and the Vp anomaly lessens) in the vicinity of the protothrusts presumably by partially draining this section prior to subduction under the lower slope (Fig. 3). The initial development of a deep décollement in the protothrusts region may not be sustainable due to the lack of a weak horizon within the deep pelagic sequences, and may fail to continue to develop once these protothrusts drain fluids out of the deeper horizons. This appears to be a rare, localized effect, since our other lines, including other areas with fracture zones (Guafo FZ, Fig. 1), do not display evidence of frontal thrust ridges in the bathymetry, deeply penetrating thrusts within profiles, or large negative Vp anomalies. The bathymetry data show only one other possible narrow region of frontal ridges in our study area near the Chiloe FZ ($\sim$41.7°), but there are no seismic lines to indicate if there are associated thrusts. Tréhu et al. (2019), in a region north of our study area, demonstrate that observations of ridges formed by protothrusts in swath bathymetry data are not enough to infer how much sediment accretion or subduction is occurring. In either case, the effect appears to be localized since it does not appear on other lines, and may not affect the long-term position of the décollement.

There is little drilling data in the incoming sediment section to provide ground truth to our observations; however, what does exist supports the hypothesis that the trench sediment has effective drainage. Along the entire Chile margin, the incoming sediment sequence consists of only 30–150 m of pelagic sediments on top of the incoming plate (Kudrass et al., 1998). Consequently, thick pelagic and hemipelagic sequences that we presume are clay-rich, low-permeability sediment are largely lacking in the Chile trench. The bulk of the $\sim$1.6–2.9 km of trench sediment consists of recently deposited trench turbidites (Mix et al., 2003; Völker et al., 2013). ODP Site 1232 in south-central Chile (Fig. 1) recovered $\sim$371 m of sandy turbidite sequences, consisting of one lithologic unit, $\sim$70 km seaward of the trench (Mix et al., 2003). The coarse turbidite sands are numerous, averaging 2.7 coarse layers/m, and may provide ample permeable fluid pathways relative to other subduction zone trenches. The sand layers could facilitate drainage and explain localized positive residual Vp observed in trench sediment (Kulm and Woollard, 1981; Mix et al., 2003). The strength of the sediments offshore Chile could be similar to the strong, dehydrated sediment found off the coast of Sumatra (Geersen et al., 2013; Gulick et al., 2011); however, evidence of a high-fluid-pressure proto-décollement has been found in Sumatra, which does not appear to be present in south-central Chile (Geersen et al., 2013; Hüpers et al., 2017). Along Chile, the trench sediments are transported along-strike by an axial channel mainly to the north as the seafloor becomes deeper (Völker et al., 2013), which creates a thick, trench turbidite section along the entire segment of the margin that may not contain regions of overpressure or localized weak layers. These conditions lead to the shallowest sediments being the most mechanically weak, resulting in the formation of the shallow décollement (Le Pichon et al., 1993).

4.3. Relationship to megathrust earthquakes

The position of the décollement well above the subducting topography limits the development of possible heterogeneities along the plate interface. These observations are consistent with mechanisms for the margin-wide locking at depth during interseismic periods (Ruff, 1989; Scholl et al., 2015), because the sediments cover the topography on the down-going plate and prevent interactions with the upper plate that localize stresses and trigger ruptures (Mochizuki et al., 2008; Wang and Bilek, 2014). This allows stress accumulation to higher levels and over broader areas than décollements that interact with rough crust. What we have yet to determine is whether the position remains shallow at greater depths or if it steps down closer to the top of the crust. Studies of mass balance along the Chile margin do provide some broad constraints on total accretion. Although subduction has occurred here since the late Carboniferous (Willner et al., 2004), and trench sediment levels have likely been near-constant since the Miocene (Bangs and Cande, 1997), only a very small frontal accretionary prism exists, $<$40 km wide (Bangs and Cande, 1997; Contreras-Reyes et al., 2010). Therefore, proportionally small amounts of the trench sediments have been accreted by either frontal or basal accretion (Bangs and Cande, 1997; Kukowski and Oncken, 2006) and on average, the décollement must have maintained a very shallow position at the deformation front as it is currently.

The rapid drainage and consolidation that we observe for the trench sediments may also be a factor in their frictional properties along the megathrust. The somewhat greater strength of the trench sediment may be because of the turbidite lithologies, or from unusually efficient, shallow fluid loss that lessens the potential for high-fluid pressure along the megathrust. Either of these could enhance velocity-weakening behavior at shallower depth than is typical for most subduction zones, similar to what has been suggested in Sumatra (Geersen et al., 2013; Gulick et al., 2011; Hüpers et al., 2017). These conditions are conducive to strong locking and rupture along the entire segment of the subduction zone. They may also contribute to tsunamigenesis by promoting slip closer to the trench, like what occurred during the 2011 Tohoku and 2004 Sumatra earthquakes (Geersen et al., 2013; Gulick et al., 2011; Kodaira et al., 2012; Lay et al., 2011). Rupture up to the trench has been modeled for both the Valdivia and Maule ruptures (Moreno et al., 2009; Yue et al., 2014).

Ultimately, images of the top of ocean crust and subducted sediment along the deeper, strongly locked portions of the Chile rupture areas are needed to fully assess fault conditions leading to great earthquakes. We expect to image structure beyond the toe with further work, but this is challenging in this complex setting. Projection to depths beyond the lower slope is difficult for most subduction zones and a more complete understanding of this mechanism globally is still limited. Scholl et al. (2015) noted that the 2011 Tohoku Mw $\sim$9.0 rupture occurs where there is $<$1 km of sediment on the incoming plate, so other mechanisms beyond the lower slope may have a role (Seno, 2017). Our assessment of subducted sediment thickness beyond the lower slope (Fig. 6) may also raise questions regarding other sites with great earthquakes that cannot yet be fully addressed without a more complete picture of deeper structure. However, our study does show very little frontal accretion along the south central Chile margin, and this

margin is especially prone to developing a smooth, homogeneous megathrust over a very broad region.

5. Summary

The incoming sediments along the south-central Chile margin, composed almost entirely of trench wedge turbidites, appear to be stronger and potentially better drained than sediments found in other subduction settings. This leads to almost the entire 1.6–2.9 km trench section subducting beneath the toe. Our data show an unusually shallow décollement forms along nearly 1,000 km of the south central Chile margin, and that this is unusual, compared to other subduction zones worldwide (Fig. 6, Table 1). The homogeneous, frictionally strong, and well-drained trench sediment, which results in a smooth and relatively strong plate boundary, may be responsible for the widespread strong locking between the Nazca and South American plates observed along the margin (Fig. 1), leading to large megathrust earthquakes. This study highlights that the thickness, consolidation state, and strength of the incoming sediments may exert direct control on interplate coupling and megathrust earthquake behavior, and, building on the argument by Han et al. (2017), trench and lower slope processes impact the seismogenic zone by controlling sediment partitioning past the toe. Our results also point out that this behavior is anomalous when compared to sediment-rich subduction zones worldwide where, in general, most of the incoming sediment is accreted. Regional differences in the partitioning between accreted and subducted sediment should be included in sediment recycling estimates and models of subduction zone behavior.

Declaration of competing interest

The authors declare that they have no known competing financial interests or personal relationships that could have appeared to influence the work reported in this paper.

Acknowledgements

We would like to thank the captain, crew, and science party of the R/V Marcus G. Langseth for their help in collecting data for MGL1701. This work was supported by US National Science Foundation grants OCE-1559293 and OCE-1558867. EC-R acknowledges the support of the PIA-CONICYT, grant ACT172002. Seismic data processing and interpretation were completed using the Paradigm processing software packages Echos and Geodepth. Data used in this study are publicly available from the Marine Geoscience Data System (http://www.marine-geo.org/index.php).

Appendix A. Supplementary material

Supplementary material related to this article can be found online at https://doi.org/10.1016/j.epsl.2020.116195.

References

Arnulf, A.F., Singh, S.C., Harding, A.J., Kent, G.M., Crawford, W., 2011. Strong seismic heterogeneity in layer 2A near hydrothermal vents at the Mid-Atlantic Ridge. Geophys. Res. Lett. 38.

Arnulf, A.F., Harding, A.J., Kent, G.M., Wilcock, W.S.D., 2018. Structure, seismicity, and accretionary processes at the hot spot-influenced Axial Seamount on the Juan de Fuca Ridge. J. Geophys. Res., Solid Earth 123, 4618–4646. https://doi.org/10.1029/2017JB015131.

Bangs, N.L., Shipley, T.H., Gulick, S.P.S., Moore, G.F., Kuromoto, S., Nakamura, Y., 2004. Evolution of the Nankai Trough décollement from the trench into the seismogenic zone: inferences from three-dimensional seismic reflection imaging. Geology 32, 273–276.

Bangs, N.L.B., Cande, S.C., 1997. Episodic development of a convergent margin inferred from structures and processes along the southern Chile margin. Tectonics 16, 489–503. https://doi.org/10.1029/97TC00494.

Bangs, N.L.B., Westbrook, G.K., Ladd, J.W., Buhl, P., 1990. Seismic velocities from the Barbados Ridge complex: indicators of high pore fluid pressures in an accretionary complex. J. Geophys. Res. 95, 8767–8782. https://doi.org/10.1029/JB095iB06p08767.

Bangs, N.L.B., Gulick, S.P.S., Shipley, T.H., 2006. Seamount subduction erosion in the Nankai Trough and its potential impact on the seismogenic zone. Geology 34, 701–704. https://doi.org/10.1130/G22451.1.

Bangs, N.L.B., Moore, G.F., Gulick, S.P.S., Pangborn, E.M., Tobin, H.J., Kuramoto, S., Taira, A., 2009. Broad, weak regions of the Nankai Megathrust and implications for shallow coseismic slip. Earth Planet. Sci. Lett. 284, 44–49. https://doi.org/10.1016/j.epsl.2009.04.026.

Barnes, P.M., Ghisetti, F.C., Ellis, S., Morgan, J.K., 2018. The role of protothrusts in frontal accretion and accommodation of plate convergence, Hikurangi subduction margin, New Zealand. Geosphere 14, 440–468. https://doi.org/10.1130/GES01552.1.

Behrmann, J.H., Kopf, A., 2001. Balance of tectonically accreted and subducted sediment at the Chile triple junction. Int. J. Earth Sci. 90, 753–768. https://doi.org/10.1007/s005310000172.

Bray, C.J., Karig, D.E., Sciences, G., 1986. Physical properties of sediments from the Nankai Trough, Deep Sea Drilling Project Leg 87A, Sites 582 and 583. Initial Rep. Deep Sea Drill. Proj. 87, 827–842.

Cifuentes, I.L., 1989. The 1960 Chilean earthquakes. J. Geophys. Res. 94, 665. https://doi.org/10.1029/JB094iB01p00665.

Cochrane, G.R., Moore, J.C., Mackay, M.E., Moore, G.F., 1994. Velocity and inferred porosity model of the Oregon accretionary prism for multichannel seismic reflection data: implications on sediment dewatering and overpressure. J. Geophys. Res. 99, 7033–7043. https://doi.org/10.1029/93JB03206.

Contreras-Reyes, E., Carrizo, D., 2011. Control of high oceanic features and subduction channel on earthquake ruptures along the Chile-Peru subduction zone. Phys. Earth Planet. Inter. 186, 49–58. https://doi.org/10.1016/j.pepi.2011.03.002.

Contreras-Reyes, E., Flueh, E.R., Grevemeyer, I., 2010. Tectonic control on sediment accretion and subduction off south central Chile: implications for coseismic rupture processes of the 1960 and 2010 megathrust earthquakes. Tectonics 29. https://doi.org/10.1029/2010TC002734.

Davis, D.M., von Huene, R., 1987. Inferences on sediment strength and fault friction from structures at the Aleutian Trench. Geology 15, 517–522. https://doi.org/10.1130/0091-7613(1987)152.0.CO;2.

Dean, S.M., McNeill, L.C., Henstock, T.J., Bull, J.M., Gulick, S.P.S.S., Austin, J.A., Bangs, N.L.B.B., Djajadihardja, Y.S., Permana, H., 2010. Contrasting decollement and prism properties over the Sumatra 2004-2005 earthquake rupture boundary. Science 80 (329), 207–210. https://doi.org/10.1126/science.1189373.

Díaz-Naveas, J.L., 1999. Sediment Subduction and Accretion at the Chilean Convergent Margin, Between 35° and 40°S. Christian-Albrechts-Universität.

Eakin, D.H., 2014. An Analysis of Subduction Related Tectonics Offshore Southern and Eastern Taiwan.

Erickson, S.N., Jarrard, R.D., 1998. Velocity-porosity relationships for water-saturated siliciclastic sediments. J. Geophys. Res., Solid Earth 103, 30385–30406. https://doi.org/10.1029/98JB02128.

Geersen, J., Behrmann, J.H., Krastel, S., Ranero, C.R.C.R., Diaz-Naveas, J., Weinrebe, W., Völker, D., Krastel, S., Ranero, C.R.C.R., Diaz-Naveas, J., Weinrebe, W., 2011. Active tectonics of the South Chilean marine fore arc (35°S-40°S). Tectonics 30, 1–16. https://doi.org/10.1029/2010TC002777.

Geersen, J., McNeill, L., Henstock, T.J., Gaedicke, C., 2013. The 2004 Aceh-Andaman Earthquake: early clay dehydration controls shallow seismic rupture. Geochem. Geophys. Geosyst. 14, 3315–3323. https://doi.org/10.1002/ggge.20193.

Gulick, S.P.S., Austin, J.A., McNeill, L.C., Bangs, N.L.B., Martin, K.M., Henstock, T.J., Bull, J.M., Dean, S., Djajadihardja, Y.S., Permana, H., 2011. Updip rupture of the 2004 Sumatra earthquake extended by thick indurated sediments. Nat. Geosci. 4, 453–456. https://doi.org/10.1038/ngeo1176.

Han, S., Bangs, N.L.B., Carbotte, S.M., Saffer, D.M., Gibson, J.C., 2017. Links between sediment consolidation and Cascadia megathrust slip behaviour. Nat. Geosci. 10, 954–959. https://doi.org/10.1038/s41561-017-0007-2.

Heuret, A., Conrad, C.P., Funiciello, F., Lallemand, S., Sandri, L., 2012. Relation between subduction megathrust earthquakes, trench sediment thickness and upper plate strain. Geophys. Res. Lett. 39, 1–7. https://doi.org/10.1029/2011GL050712.

Hüpers, A., Torres, M.E., Owari, S., McNeill, L.C., Dugan, B., Henstock, T.J., Milliken, K.L., Petronotis, K.E., Backman, J., Bourlange, S., Chemale, F., Chen, W., Colson, T.A., Frederik, M.C.G., Guèrin, G., Hamahashi, M., House, B.M., Jeppson, T.N., Kachovich, S., Kenigsberg, A.R., Kuranaga, M., Kutterolf, S., Mitchison, F.L., Mukoyoshi, H., Nair, N., Pickering, K.T., Pouderoux, H.F.A., Shan, Y., Song, I., Vannucchi, P., Vrolijk, P.J., Yang, T., Zhao, X., 2017. Release of mineral-bound water prior to subduction tied to shallow seismogenic slip off Sumatra. Science 80 (356), 841–844. https://doi.org/10.1126/science.aal3429.

Jaeger, J.C., Cook, N.G.W., 1969. Fundamentals of Rock Mechanics. Methuen & Co. Ltd., London, p. 513.

Kodaira, S., No, T., Nakamura, Y., Fujiwara, T., Kaiho, Y., Miura, S., Takahashi, N., Kaneda, Y., Taira, A., 2012. Coseismic fault rupture at the trench axis during the 2011 Tohoku-oki earthquake. Nat. Geosci. 5, 646–650. https://doi.org/10.1038/ngeo1547.

Kopf, A., Brown, K.M., 2003. Friction experiments on saturated sediments and their implications for the stress state of the Nankai and Barbados subduction thrusts. Mar. Geol. 202, 193–210. https://doi.org/10.1016/S0025-3227(03)00286-X.

Kopp, C., Fruehn, J., Flueh, E.R., Reichert, C., Kukowski, N., Bialas, J., Klaeschen, D., 2000. Structure of the Makran subduction zone from wide-angle and reflection seismic data. Tectonophysics 329, 171–191. https://doi.org/10.1016/S0040-1951(00)00195-5.

Kopp, H., Hindle, D., Klaeschen, D., Oncken, O., Reichert, C., Scholl, D., 2009. Anatomy of the western Java plate interface from depth-migrated seismic images. Earth Planet. Sci. Lett. 288, 399–407. https://doi.org/10.1016/J.EPSL.2009.09.043.

Kudrass, H.R., Von Rad, U., Seyfied, H., Andruleit, H., Hinz, K., Reichert, C., 1998. Age and facies of sediments of the northern Chilean continental slope-Evidence for intense vertical movements. In: Crustal Investig. Off- and Onshore Nazca/CINCA, pp. 170–196.

Kukowski, N., Oncken, O., 2006. Subduction erosion — the "normal" mode of fore-arc material transfer along the Chilean Margin? In: The Andes. Springer Berlin Heidelberg, pp. 217–236.

Kulm, L.D., Woollard, G.P., 1981. Nazca Plate: Crustal Formation and Andean Convergence: A Volume Dedicated to George P. Woollard. Geological Society of America.

Lay, T., Ammon, C.J., Kanamori, H., Xue, L., Kim, M.J., 2011. Possible large near-trench slip during the 2011Mw 9.0 off the Pacific coast of Tohoku Earthquake. Earth Planets Space 63, 687–692. https://doi.org/10.5047/eps.2011.05.033.

Le Pichon, X., Henry, P., Lallemant, S., 1993. Accretion and erosion in subduction zones: the role of fluids. Annu. Rev. Earth Planet. Sci. 21, 307–331.

Lester, R., McIntosh, K., Van Avendonk, H.J.A., Lavier, L., Liu, C.-S., Wang, T.K., 2013. Crustal accretion in the Manila trench accretionary wedge at the transition from subduction to mountain-building in Taiwan. Earth Planet. Sci. Lett. 375, 430–440. https://doi.org/10.1016/J.EPSL.2013.06.007.

Li, J., Shillington, D.J., Saffer, D.M., Bécel, A., Nedimović, M.R., Kuehn, H., Webb, S.C., Keranen, K.M., Abers, G.A., 2018. Connections between subducted sediment, pore-fluid pressure, and earthquake behavior along the Alaska megathrust. Geology 46, 299–302. https://doi.org/10.1130/G39557.1.

Marcaillou, B., Collot, J.Y., Ribodetti, A., d'Acremont, E., Mahamat, A.A., Alvarado, A., 2016. Seamount subduction at the North-Ecuadorian convergent margin: effects on structures, inter-seismic coupling and seismogenesis. Earth Planet. Sci. Lett. 433, 146–158. https://doi.org/10.1016/j.epsl.2015.10.043.

Mix, A.C., Tiedemann, R., Blum, P., Abrantes, F.F., Benway, H., Cacho-Lascorz, I., Chen, M.T., Delaney, M.L., 2003. Proceedings of the Ocean Drilling Program, 202 Initial Reports. Proceedings of the Ocean Drilling Program, Part A: Initial Reports. Ocean Drilling Program, College Station, TX, United States.

Mochizuki, K., Yamada, T., Shinohara, M., Yamanaka, Y., Kanazawa, T., 2008. Weak interface coupling by seamounts and repeating M∼7 earthquakes. Science 80 (321), 1194–1197. https://doi.org/10.1126/science.1160250.

Moeremans, R., Singh, S.C., Mukti, M., McArdle, J., Johansen, K., 2014. Seismic images of structural variations along the deformation front of the Andaman-Sumatra subduction zone: implications for rupture propagation and tsunamigenesis. Earth Planet. Sci. Lett. 386, 75–85. https://doi.org/10.1016/j.epsl.2013.11.003.

Moore, G.F., Shipley, T.H., Stoffa, P.L., Karig, D.E., Taira, A., Kuramoto, S., Tokuyama, H., Suyehiro, K., 1990. Structure of the Nankai Trough Accretionary Zone from multichannel seismic reflection data. J. Geophys. Res. 95, 8753. https://doi.org/10.1029/JB095iB06p08753.

Moore, G.F., Park, J.-O., Bangs, N.L., Gulick, S.P., 2009. Structural and Seismic Stratigraphic Framework of the NanTroSEIZE Stage 1 Transect.

Moreno, M., Rosenau, M., Oncken, O., 2010. 2010 Maule earthquake slip correlates with pre-seismic locking of Andean subduction zone. Nature 467, 198–202. https://doi.org/10.1038/nature09349.

Moreno, M., Melnick, D., Rosenau, M., Bolte, J., Klotz, J., Echtler, H., Baez, J., Bataille, K., Chen, J., Bevis, M., Hase, H., Oncken, O., 2011. Heterogeneous plate locking in the south-central Chile subduction zone: building up the next great earthquake. Earth Planet. Sci. Lett. 305, 413–424. https://doi.org/10.1016/j.epsl.2011.03.025.

Moreno, M.S., Bolte, J., Klotz, J., Melnick, D., 2009. Impact of megathrust geometry on inversion of coseismic slip from geodetic data: application to the 1960 Chile earthquake. Geophys. Res. Lett. 36, 1–6. https://doi.org/10.1029/2009GL039276.

Morgan, J.K., Bangs, N.L., 2017. Recognizing seamount-forearc collisions at accretionary margins: insights from discrete numerical simulations. Geology 45, 635–638. https://doi.org/10.1130/G38923.1.

Morgan, J.K., Karig, D.E., 1995. Decollement processes at the Nankai accretionary margin, southeast Japan: propagation, deformation, and dewatering. J. Geophys. Res. 100, 15221–15231. https://doi.org/10.1029/95JB00675.

Nasu, N., Tomoda, Y., Kobayashi, K., Kagami, H., 1982. Multi-channel seismic reflection data across Nankai Trough. In: IPOD-Japan Basic Data Series, No. 4. Ocean Research Institute, University of Tokyo, Tokyo.

Park, J.O., Tsuru, T., Kodaira, S., Cummins, P.R., Kaneda, Y., 2002. Splay fault branching along the Nankai subduction zone. Science 80 (297), 1157–1160. https://doi.org/10.1126/science.1074111.

Pedley, K.L., Barnes, P.M., Pettinga, J.R., Lewis, K.B., 2010. Seafloor structural geomorphic evolution of the accretionary frontal wedge in response to seamount subduction, Poverty Indentation, New Zealand. Mar. Geol. 270, 119–138. https://doi.org/10.1016/j.margeo.2009.11.006.

Plafker, G., Savage, J.C., 1970. Mechanism of the Chilean earthquakes of May 21 and 22, 1960. Bull. Geol. Soc. Am. 81, 1001–1030. https://doi.org/10.1130/0016-7606(1970)81[1001:MOTCEO]2.0.CO;2.

Ruff, L.J., 1989. Do trench sediments affect great earthquake occurrence in subduction zones? Pure Appl. Geophys. PAGEOPH 129, 263–282. https://doi.org/10.1007/BF00874629.

Scherwath, M., Contreras-Reyes, E., Flueh, E.R., Grevemeyer, I., Krabbenhoeft, A., Papenberg, C., Petersen, C.J., Weinrebe, R.W., 2009. Deep lithospheric structures along the southern central Chile margin from wide-angle P-wave modelling. Geophys. J. Int. 179, 579–600. https://doi.org/10.1111/j.1365-246X.2009.04298.x.

Scholl, D.W., Kirby, S.H., von Huene, R., Ryan, H., Wells, R.E., Geist, E.L., 2015. Great (≥Mw8.0) megathrust earthquakes and the subduction of excess sediment and bathymetrically smooth seafloor. Geosphere 11, 236–265. https://doi.org/10.1130/GES01079.1.

Seno, T., 2017. Subducted sediment thickness and Mw 9 earthquakes. J. Geophys. Res. Solid Earth 122, 470–491. https://doi.org/10.1002/2016JB013048.

Sick, C., Yoon, M.-K., Rauch, K., Buske, S., Lüth, S., Araneda, M., Bataille, K., Chong, G., Giese, P., Krawczyk, C., Mechie, J., Meyer, H., Oncken, O., Reichert, C., et al., 2006. Seismic images of accretive and erosive subduction zones from the Chilean Margin. In: Oncken, O., Chong, G., Franz, G., Giese, P., Götze, H.-J., Ramos, V.A., Strecker, M.R., Wigger, P. (Eds.), The Andes: Active Subduction Orogeny. Springer Berlin Heidelberg, Berlin, Heidelberg, pp. 147–169.

Tréhu, A.M., Blakely, R.J., Williams, M.C., 2012. Subducted seamounts and recent earthquakes beneath the central cascadia forearc. Geology 40, 103–106. https://doi.org/10.1130/G32460.1.

Tréhu, A.M., Hass, B., DeMoor, A., Maksymowicz, A., Contreras-Reyes, E., Vera, E., Tryon, M.D., 2019. Insights into controls on up-dip and along-strike propagation of slip during subduction zone earthquakes from a high-resolution seismic reflection survey across the northern limit of slip during the 2010 Mw8.8 Maule earthquake. Geosphere 15 (6), 1751–1773.

Völker, D., Geersen, J., Contreras-Reyes, E., Reichert, C., 2013. Sedimentary fill of the Chile Trench (32-46°S): volumetric distribution and causal factors. J. Geol. Soc. (Lond.) 170, 723–736. https://doi.org/10.1144/jgs2012-119.

von Huene, R., Miller, J.J., Weinrebe, W., 2012. Subducting plate geology in three great earthquake ruptures of the western Alaska margin, Kodiak to Unimak. Geosphere 8, 628–644. https://doi.org/10.1130/GES00715.1.

von Huene, R., Miller, J.J., Krabbenhoeft, A., 2019. The Shumagin seismic gap structure and associated tsunami hazards, Alaska convergent margin. Geosphere 15, 324–341. https://doi.org/10.1130/GES01657.1.

Wang, K., Bilek, S.L., 2014. Invited review paper: fault creep caused by subduction of rough seafloor relief. Tectonophysics 610, 1–24. https://doi.org/10.1016/j.tecto.2013.11.024.

Willner, A.P., Glodny, J., Gerya, T.V., Godoy, E., Massonne, H.-J., 2004. A counterclockwise PTt path of high-pressure/low-temperature rocks from the Coastal Cordillera accretionary complex of south-central Chile: constraints for the earliest stage of subduction mass flow. Lithos 75, 283–310. https://doi.org/10.1016/J.LITHOS.2004.03.002.

Ye, L., Kanamori, H., Lay, T., 2018. Global variations of large megathrust earthquake rupture characteristics. Sci. Adv. 4. https://doi.org/10.1126/sciadv.aao4915.

Yue, H., Lay, T., Rivera, L., An, C., Vigny, C., Tong, X., Soto, J.C.B., 2014. Localized fault slip to the trench in the 2010 Maule, Chile Mw = 8.8 earthquake from joint inversion of high-rate GPS, teleseismic body waves, InSAR, campaign GPS, and tsunami observations. J. Geophys. Res., Solid Earth 119, 7786–7804. https://doi.org/10.1002/2014JB011340.